ECE5340 - Final Report for an Aluminum Oxide - Silicon Oxide TE Mode Converter

Mads Peter Berg,[1] Francis Chen,[1] and Jeffrey Wilcox[2]
[1)] *Department of Applied and Engineering Physics, Cornell University.*
[2)] *Department of Electrical and Computer Engineering, Cornell University.*

(Dated: 12 May 2023)

We present a design for a compact, low-cost single-waveguide TE0-TE1 mode converter for 658 nm light, primarily purposed towards bimodal interferometry chip-integrated devices seen within the fields of biosensing. The goal is to achieve perfect 50/50 percent splitting of the power of the two modes. The waveguide is comprised of an Al_2O_3 core with SiO_2 (glass) cladding. The device length is no more than 100 µm in length, and depending on the width of the cladding, no more than several µm in width. Our design is tested in simulation via the Beam Propagation Method as well as FDTD simulations, with a conversion efficiency from the fundamental mode to the first order excited mode approaching 50%. We show simulation results while varying both the depth (amplitude) fo the sinusoidal grating as well as the number of periods the grating lasts along the propagation axis, and show the underlying analytical calculations for the design parameters that we hold fixed.

I. INTRODUCTION & MOTIVATIONS

The fields of biosensing have seen the demand to identify particles of a specific chemical composition within a given sample (referred to as an analyte). Integrated optical devices (IO devices) are desirable as lab-on-a-chip (LOC) biosensors for several reasons, such as their compactness, high sensitivity, mechanical stability[1]. Within IO devices, several methods of biosensing have seen widespread use of environment monitoring and medical diagnostics. These all operate on the principle method of evanescent field detection. This principle relies on the molecular interaction between the analyte with given bioreceptors within the sample, which variably alters the index of refraction n_{sample}.

Our simulation-implemented design takes after a bimodal waveguide interferometer (BiMW). The principle of operation of such a sensor relies on the interference between the fundamental and first TE or TM modes within a straight waveguide. Light launched into the waveguide takes on the form of a Gaussian profile (or that of the TE fundamental mode). After propagating for a set distance, the guided mode reaches a section of the waveguide sporting a sinusoidal grating perturbation on one side that splits the power of the guided mode into the fundamental and the first order modes, which propagate until the device output.

II. PRINCIPLES OF OPERATION

A. Analytical Design Calculations

Multiple degrees of freedom were considered for the design of the mode-converter. These included:

- The waveguide normalized thickness V and width d.
- The effective refractive index n_{eff} (via choice of the core and cladding materials).
- The amplitude of the grating perpendicular to the propagation axis d_g.
- The waveform of the perturbative grating ($\sin(x)$).
- The grating period along the propagation axis Λ.
- The length of the grating along the propagation axis L.

While a trench waveguide consisting of a large rectangular section of the core being replaced with the cladding material could in theory represent an anti-symmetric perturbation which would integrate with the odd functional modes of the waveguide (the first excited mode in particular), the loss associated with such a large perturbation would likely cause most of the power to radiate out of the waveguide, thus leading to an inefficient waveguide. Furthermore, early BPM simulations showed a small amount of power transfer to the first order excited, mode, but a vanishing amount of power remaining within the fundamental mode, thus defeating the original biosensing-based purpose of a single-waveguide partial mode converter. Thus, a sinusoidal grating with a relatively small grating amplitude was decided on for the perturbing grating.

To decide on the width of the waveguide, we decided on a quantity that would only allow for two transverse modes (thickness between $m = 1$ and $m = 2$, originally assumed only slightly larger than the $m = 1$ case). Thus, the thickness was derived as follows:

$$V = \frac{2\pi}{\lambda} d \sqrt{n_1^2 - n_2^2} \tag{1}$$

$$V_c^m = m\pi \tag{2}$$

Similarly, to calculate the optimal grating period Λ, we use the phase-matching difference of the incident fundamental waveguide propagation constant β_0 with the propagation constant of the first order excited wave β_1:

$$\Lambda = -q\frac{2\pi}{\Delta\beta} = \frac{2\pi}{\beta_0 - \beta_1} \tag{3}$$

The perturbation to the mode dynamics within the waveguide would remain small so long as the grating amplitude would be much smaller than the parameter $\frac{\lambda}{n_1}$. This value would be tuned later on (see Section III B), along with the number of grating periods (equivalent to tuning the length of the grating along the propagation axis, L). These parameters were tuned while comparing the results in BPM and FDTD simulations, to determine the optimal value splitting the power propagating in the waveguide equally between the fundamental and first-order modes.

$$d_g << \frac{\lambda}{n_1} \rightarrow \kappa = \frac{h_0 h_1}{\sqrt{\beta_0 \beta_1 d_0^E d_1^E}} \frac{d_g}{4} \tag{4}$$

III. BPM SIMULATIONS AND DESIGN

The field intensities and conversion efficiencies of the mode converter were simulated via the beam propagation method, using the Crank-Nicolson method, written as an implicit Runge–Kutta method of simulating the second-order differential equations in time. These were implemented in MATLab from a template made by Professor Mehta, which featured the built-in iterative differential equation simulation code. Additionally, an absorbing rectangular layer was implemented to prevent reflections at the boundaries of the $2D$ simulated areas.

A. BPM Implementation of Asymmetric Grating

To modify the code to fit our intended waveguide design, a $2D$ array was created as follows:

- An $2D$ $N_z \times N_x$ array of points is defined, with all values set to the cladding index n_{cladding}.
- At every point in z where the grating is in effect, the baseline width is added with the amplitude of the grating per the equation:

$$A(z) = d_g(\sin(\omega_g \Delta z(z\prime - z_0\prime + 0.5)) \tag{5}$$

  Where the spatial-dependent grating deviation from the baseline width is denoted by $A(z)$, and d_g is the grating amplitude. ω_g denotes the grating frequency, Δz is the discretization along z, z' refers to the discrete array index along z, and z_0' is the discrete z-point where the grating begins. A value of $0.5\Delta z$ is added to the value of the number of discrete z-points since the grating beginning to use the midpoint value of the sinusoidal function at every discretization point.

- At every point z' from z_0 until the end of the grating, if the x co-ordinate is within the range $[-\frac{d}{2}, \frac{d}{2} + A(z)]$, the local (x', z') point is set to contain the value of n_{core}.

Later on, within the loop in the BPM code, the $1D$ array along x for a given z point, `n_Input_WG`, is replaced with the modified array `n_Sin_WG`, a slice of the $2D$ array specified above. The code is then run to generate the simulation results.

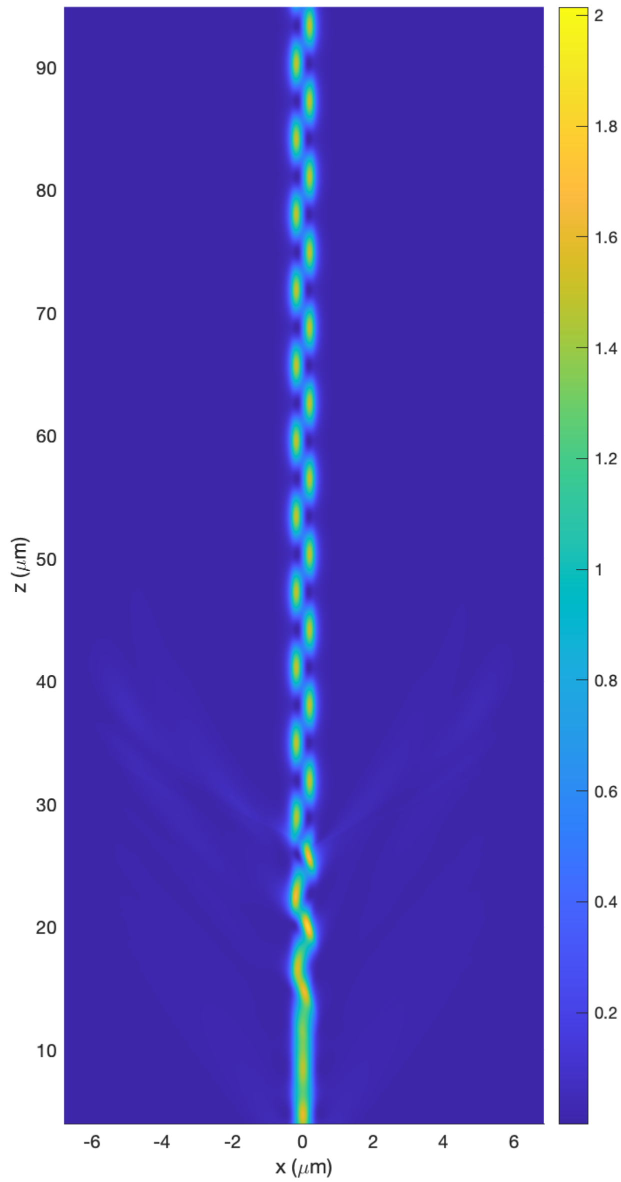

FIG. 1. **BPM field intensities as a function of** x, z**.** The grating begins at 11.0 μm, which can be seen with the asymmetric field distribution across x at every point in z onwards. The x axis is stretched to show the evanescent fields where power escapes away from the waveguide into the cladding material.

```
% Index profile for WG
n_Input_WG = nCladding*ones(1, N);
n_Peak_WG = nCladding*ones(1, N);
coreinds = find((x<=inputWGWidth/2).*(x>=-
    inputWGWidth/2));
    %find returns nonzero element indices; the boolean
    expressions
    %identifies values of x for which we are in the
    waveguide core.
n_Input_WG(coreinds) = nCore; %This line sets the
    base width to the core index.

%Create Sinusoidal Grating x-profile, asymmetric:  one
    side is sinusoidal.
gratingPeriodPattern = nCladding*ones(Nzpts+1, N
```

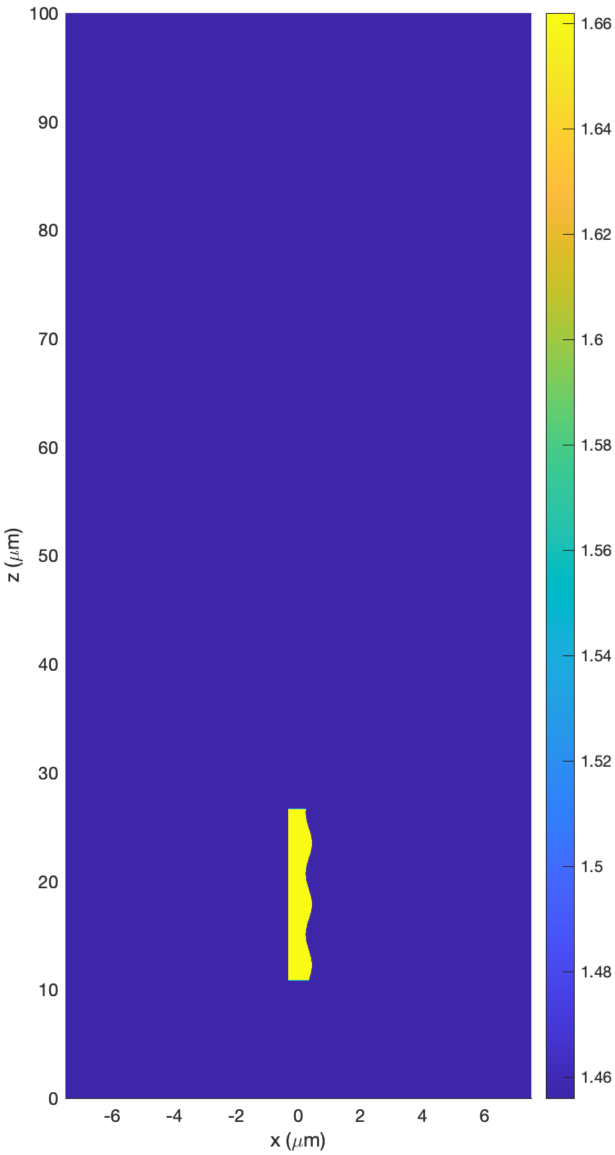

FIG. 2. **BPM visualization of the perturbative region of the asymmetric grating.** Only the grating region is highlighted in yellow here. Note that the phase of the sinusoidal grating begins at $\phi = 0$, rather than $\phi = \frac{\pi}{2}$ which would involve a gradual increase of waveguide width from the baseline width d.

```
    ); %Each slice of gratingPeriodPattern is now a
    x-profile.
for zed = gratingStart:gratingEnd
    sinusoidAmp = gratingAmp*sin(gratingFreq*
    deltaz*(zed-gratingStart+0.5));
    gratingIndsX = find((x<=inputWGWidth/2 +
    sinusoidAmp).*(x>=-inputWGWidth/2)); %Use
    midpoint rounding for Sine function.
    gratingPeriodPattern(zed, gratingIndsX) =
    nCore; %
end
```

B. BPM Simulation Results

After the grating has been implemented on top of the basic waveguide in MATLab, the BPM simulation is run, and the field intensities are plotted with respect to x, z to form a mode profile. Since the final propagating field within the waveguide would consist of a superposition of the fundamental (symmetric, positive valued) and first-order excited modes (antisymmetric, negative and positive valued), at every slice of x values for a given z co-ordinate, the final intensities should be asymmetric (see Figure 1). As expected, the simulations proved to show an asymmetric field intensity starting beginning at approximately 20 µm into the device, propagating for 80 µm until the end of the device. While the field response was not instantaneous to the grating perturbation in space, taking approximately 15 µm (approximately 2.75 periods) worth of distance along the z axis to settle into its final desired functional form, the remaining ∼80 µm worth of straight waveguide proved to be unnecessary for the purposes of mode conversion. The grating was placed offset from the beginning of the device at 0 µm to allow the wave to propagate for a short distance, allowing for the overlap integral with the fundamental mode to be performed. The $2D$ intensity plot also showed evanescent fields radiating away from the waveguide, which showed that the waveguide had some significant loss in the form of output coupling.

Our desired conversion efficiency was 50% into the fundamental mode, and 50% into the first order mode, accounting for losses that occur within the grating. This involved the generation of two arrays of the functional form of a first-order and fundamental mode fields as a function of x. The field was taken from the BPM simulation result, and a $1D$ slice was taken at every discrete point $z\prime$, which then underwent element-wise multiplication with the two generated arrays, with each element summed. The result was normalized by the sum of the array elements, thus implementing the normalized overlap integral:

$$\eta = \frac{\left| \int \vec{e} \cdot \vec{e_0}^* \, dx \right|^2}{\int \vec{e} \cdot \vec{e}^* \, dx \int \vec{e_0} \cdot \vec{e_0}^* \, dx} \tag{6}$$

Where $\vec{e_0}$ would refer to the fundamental or first-order modes given the waveguide width and effective index. Note that this integral evaluates the total power owing to a specific mode, as a fraction of the total power within the waveguide at particular cut in the propagation direction. I.e. some power may have coupled out before then, which is not captured. The result was a $1D$ array with the same length as the number of discrete $z\prime$ points. The plots of the fundamental and first-order conversion factors $\in [0, 1]$ were plotted as a function of z, shown within Figure 3.

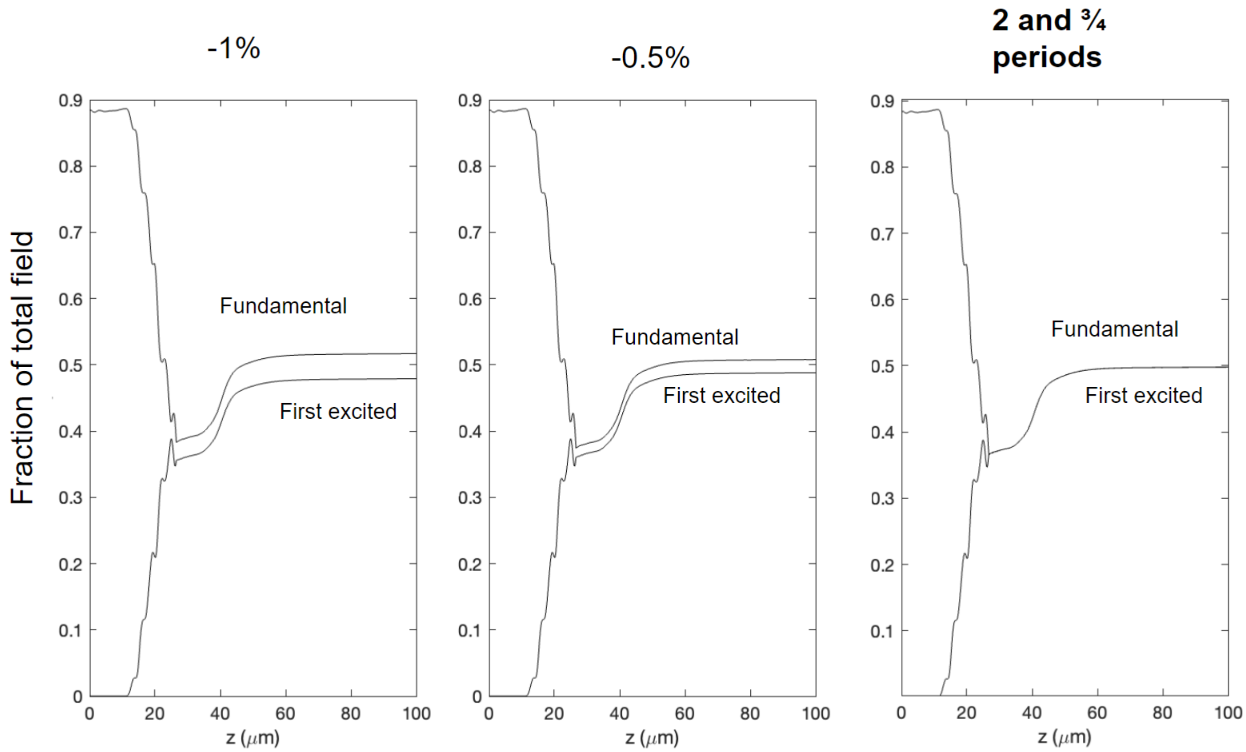

FIG. 3. **Overlap integral value as a function of propagation distance z between the simulated electric field and the field functions of the fundamental and first-order modes.** The waveguide grating length, L, was hand-tuned in order to have the overlap values approach 0.5 as closely as possible. In order of left to right, the plots show the conversion efficiencies with 99.0%, 99.5%, and 100% of the nominal value $L = 15.46\,\mu m$, corresponding the to 2.75 multiples of the period Λ.

TABLE I. Optimal Design Parameters

Parameter Name	Symbol	Value
Waveguide base width	d	0.666 39 μm
Effective refractive index	n_{eff}	1.662
Grating amplitude	d_g	0.099 29 μm
Grating period	Λ	5.622 μm
Grating length	L	15.46 μm
Input light wavelength	λ	658 nm

IV. FDTD SIMULATIONS

A. FDTD Implementation of Asymmetric Grating

After the BPM simulations showed promising results, the waveguide design was re-implemented in K-Layout, and finite-difference time-domain (FDTD) simulations were run on the new implementation. The construction of a perfect sinusoidal grating proved difficult using K-Layout, and thus the grating was once again quantized, though this time through the construction of rectangles at a total of 16 different heights (or depths) from the baseline width d, equivalent to 4-bit bit-precision. Furthermore, right-handed values were used for the heights of the rectangles, with a width Δz.

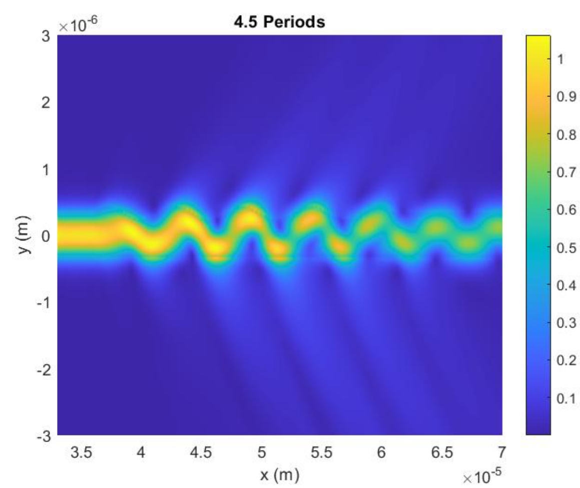

FIG. 4. FDTD simulation heatmaps of the field intensity across space, given a sinusoidal waveguide grating 4.0 periods long.

Multiple grating implementations were constructed within K-Layout for the FDTD simulations, featuring different grating lengths L, which, given the fixed spatial frequency of the grating, corresponded to different numbers of periods the sinusoidal variation would go through after starting. Two types of waveguide designs were generated: unidirectional and bidirectional grating designs. Although these distinctions do not have any direct application to the biosensing, it was important to identify whether the unidirectional devices had significant loss due to an amplitude step at the end of the grating. For this reason, two unidirectional gratings and four bidirectional gratings were designed for comparison and determination of the experimental differences in performance between different waveguide lengths. Chosen lengths were based on our BPM simulation results and selected in multiples of $\frac{1}{4}$ periods for ease of manufacturing.

B. FDTD Simulation Results

To determine the efficiency of our designs, we observed the scattering parameters of each design. S_{11} represented how much of the electric field went out the input port when an optical wave was sent into the input port, S_{21} represented how much of the electric field went out the output port in the fundamental mode when an optical wave was sent into the input port, and S_{31} represented how much of the electric field went out the output port in the excited mode when an optical wave was sent into the input port. These varied over different frequencies, but due to the biosensing application we were only concerned with those of the 658 nm. These parameters squared represent how much of the power is transferred from the input port to the respective exit of the device.

Of the six different designs, the one which achieved the closest to equal power splitting had a grating length of 3.5 periods. The 2.75 period grating was able to couple approximately 50 % of the input power into the excited mode, but there was significant loss of the fundamental mode which meant much less than 50 % of the input power was coupled into the fundamental mode leading to unequal splitting between modes. As the length was increased from 2.75 periods, there was less coupling into the excited mode as well as less loss from the fundamental so once the 3.5 period grating had almost equal power splitting, the lengths after returned to significantly unequal splitting with the fundamental mode now dominating the output. The amplitude step for the unidirectional couplers did not seem to have an effect on the power coupling as those designs closely followed a larger pattern across all the designs dependent on length.

V. DISCUSSION AND CONCLUSIONS

We have constructed a design for a single-waveguide fundamental-to-first mode converter with promising performance in BPM and FDTD simulations, while providing the estimated performance keeping in mind the possibility of defects during fabrication. Though additional testing should be performed to reconcile the differences in the optimal grating length L between the two methods of simulation, the primary objective of partial excitation of the two desired modes has been demonstrated through both methods.

While factors of loss may be less important within the fields of biosensing, it should be kept in mind that these devices will likely be produced en masse and distributed on a chip for the rapid detection of analytes within multiple samples simultaneously, thus leading to energy considerations at large enough scales. As can be seen in both simulation platforms, the large value of d_g causes every period of the grating to leak a considerable amount of power into the cladding region, thus limiting the flexibility and energy-efficiency of the mode converter. Thus, optimal grating lengths L would ideally be the smallest value wherein the conversion efficiencies cross $\eta = 50\%$.

ACKNOWLEDGMENTS

We wish to acknowledge and thank Professor Karan Mehta for providing us the opportunity to develop this device, providing us the template for the BPM code while aiding in FDTD simulations. Most of all, we'd like to thank him for his patience while guiding us in learning the necessary prerequisites to understand its operation, guiding us through references and the .

[1] D. Duval, A. B. González-Guerrero, S. Dante, J. Osmond, R. Monge, L. J. Fernández, K. E. Zinoviev, C. Domínguez, and L. M. Lechuga, "Nanophotonic lab-on-a-chip platforms including novel bimodal interferometers, microfluidics and grating couplers," Lab on a Chip **12**, 1987–1994 (2012).

[2] J.-M. Liu, *Photonic devices* (Cambridge University Press, 2009).

[3] G. L. Pedrola, *Beam propagation method for design of optical waveguide devices* (John Wiley & Sons, 2015).

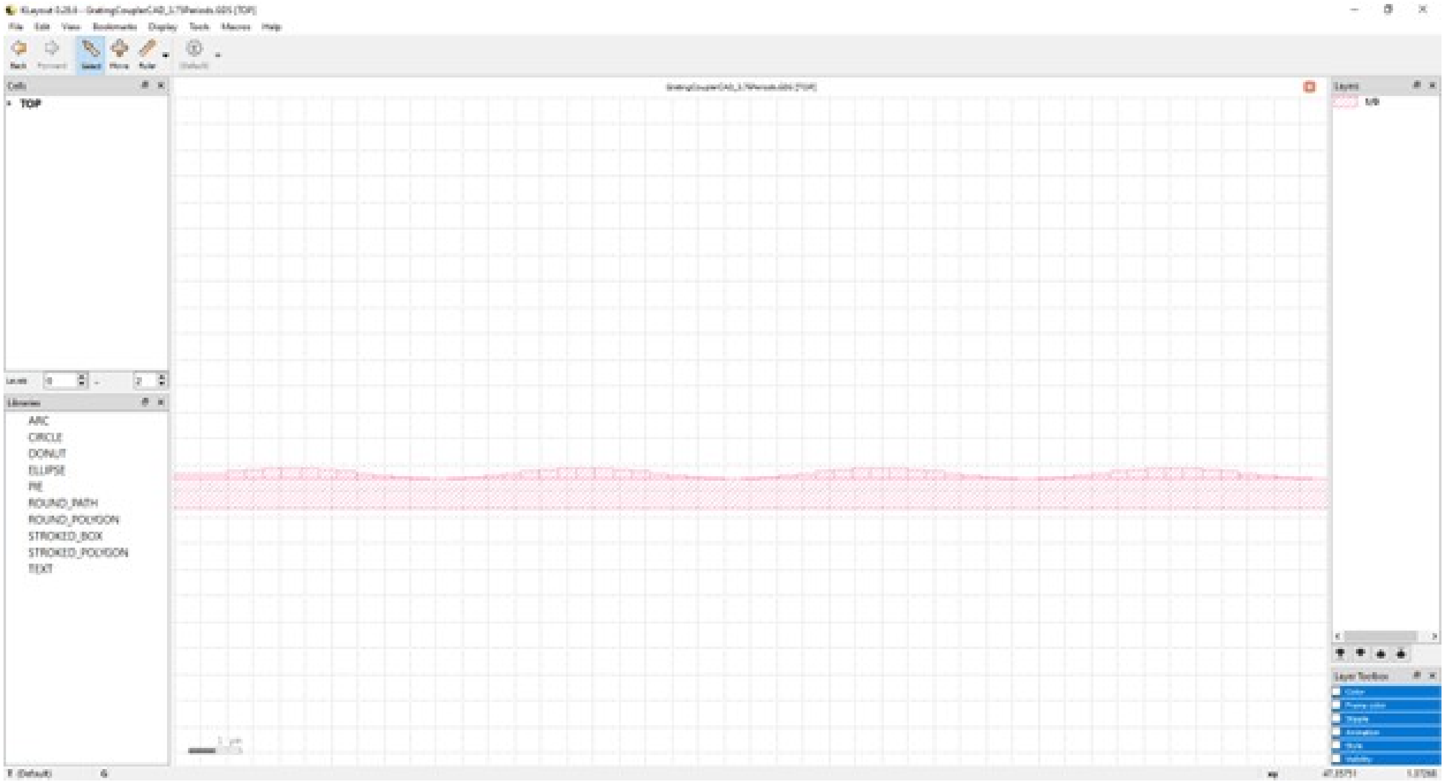

FIG. 5. Designer View of the CAD Program in KLayout. This is where the models where translated from periodic undefined refractive index changes, as used in the MATLab Beam Propagation simulation method to physical periodic width changes for the Finite Difference Time Domain simulation method. Instead of midpoint-value interpolation for the sine function, right-handed values were taken for the height of the rectangles used to construct the grating.

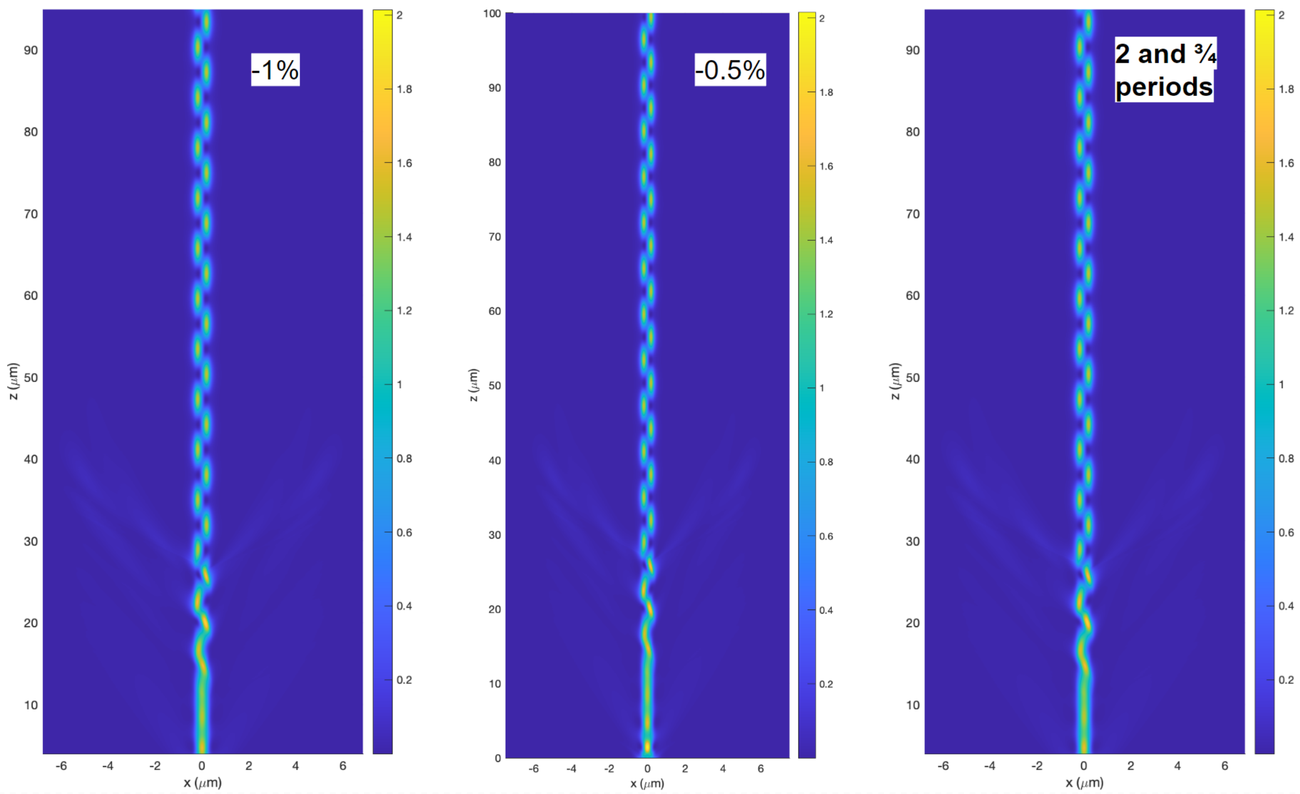

FIG. 6. BPM Simulation intensity plots generated in MATLab for a length of 2.75 periods, 0.5 % shorter, and 1 % shorter. There is generally little difference among these design behaviors, however the reflection in the 0.5 % shorter does show more reflection as can be seen by more intermittent yet brighter spots at the input port on the intensity map.

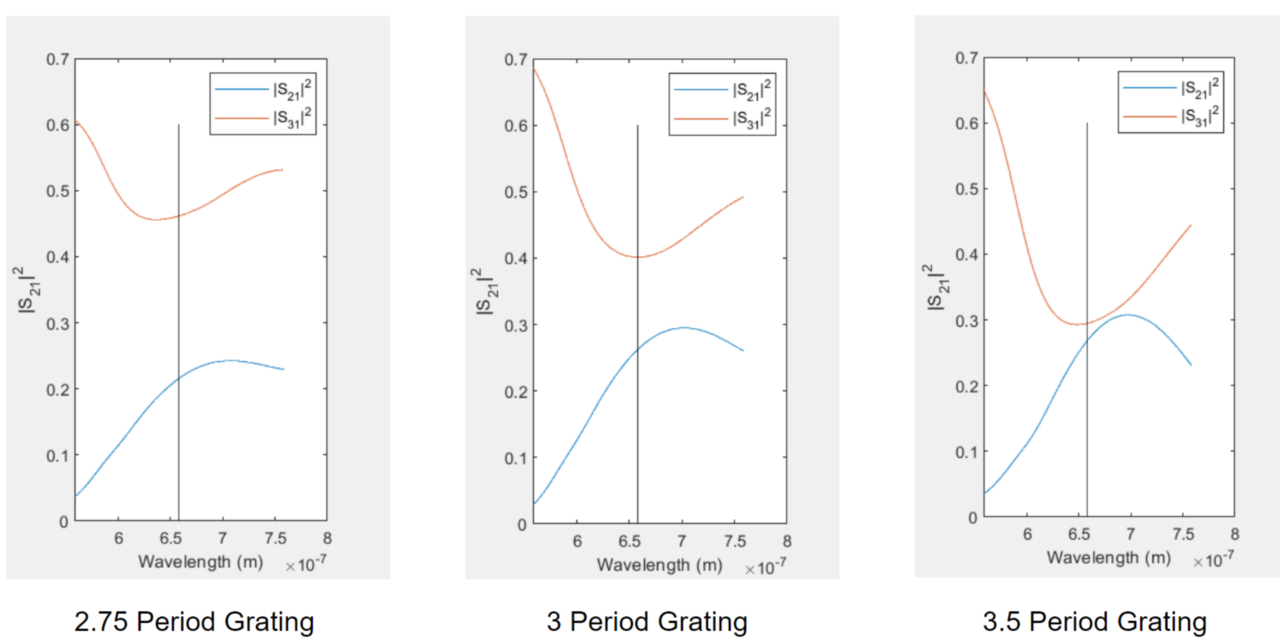

FIG. 7. Plots for the scattering parameters $|S_{21}|^2$ and $|S_{31}|^2$ in the smaller three designs to represent the fraction of power transmitted from the input to the different output modes as described in IV B over a range of wavelengths. The desired wavelength is indicated by the vertical line and $|S_{11}|^2$ is omitted as it was equal to zero for all device designs at the desired wavelength.

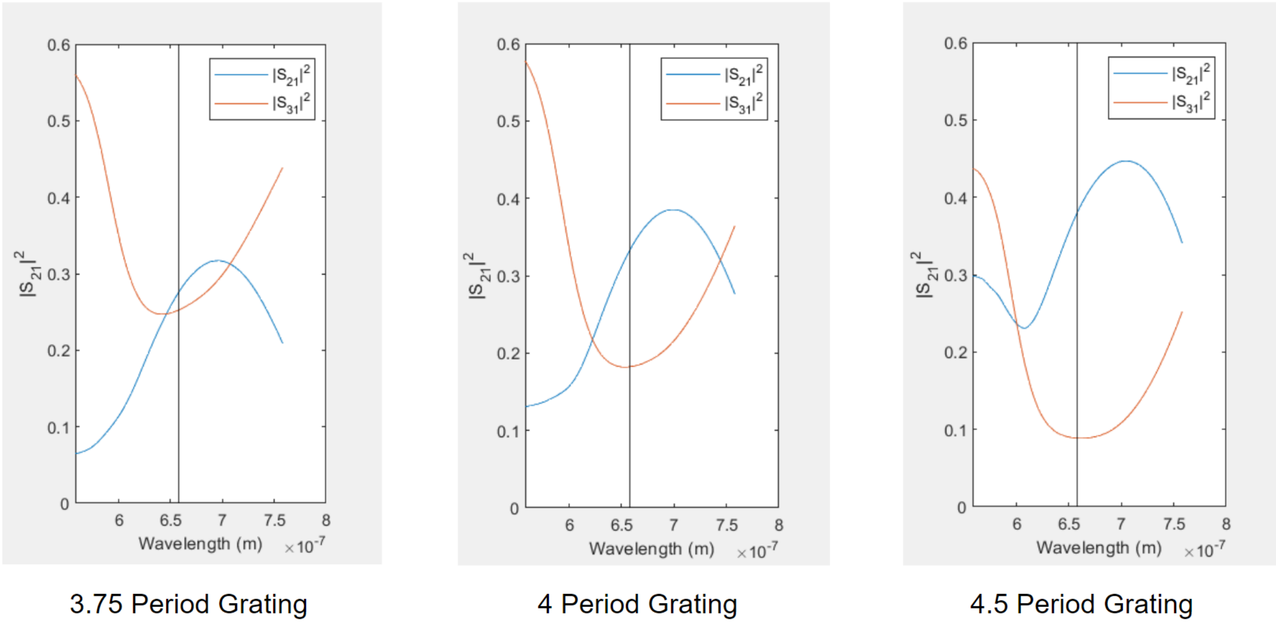

FIG. 8. Plots for the scattering parameters $|S_{21}|^2$ and $|S_{31}|^2$ in the larger three designs to represent the fraction of power transmitted from the input to the different output modes as described in IV B over a range of wavelengths. The desired wavelength is indicated by the vertical line and $|S_{11}|^2$ is omitted as it was equal to zero for all device designs at the desired wavelength.

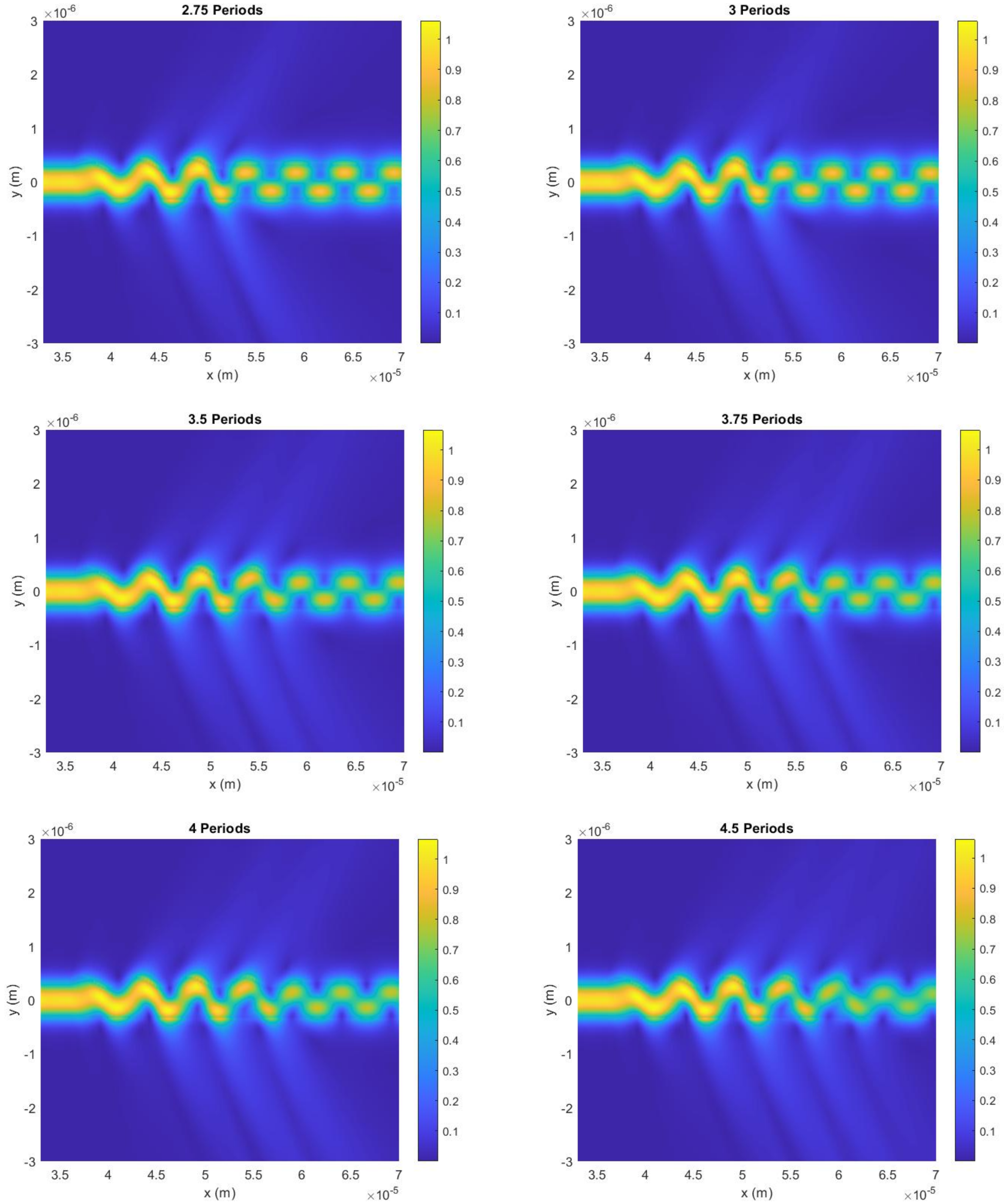

FIG. 9. **FDTD field intensities with respect to** x **(expressed here as** y**) and** z **(labelled here as** x**).** Unlike in Figure 1 plots show the field intensities specifically within the region where the grating is present, leaving out the rest of the device. Note that each peak and trough of the grating causes a evanescent field to radiate out of the waveguide, thus making shorter gratings more desirable.